# COMPUTATIONAL/EXPERIMENTAL AEROELASTIC STUDY FOR AN ALL-MOVABLE HORIZONTAL TAIL WITH TORSION FREE-PLAY

Xinyu Ai<sup>1</sup>, Xiangyan Chen<sup>1</sup>, Weiji Wang<sup>1</sup>, Jun Liu<sup>1</sup>, Xiaojia Ran<sup>1</sup> & Wei Qian<sup>1,2,3</sup>

<sup>1</sup>School of Mechanics and Aerospace Engineering, Dalian University of Technology, Dalian 116023, China <sup>2</sup>State Key Laboratory of Structural Analysis for Industrial Equipment, Dalian University of Technology, Dalian 116023, China

<sup>3</sup>Advanced Technology for Aerospace Vehicles of Liaoning Province, Dalian University of Technology, Dalian 116023, China

## **Abstract**

The free-play-induced complex nonlinear dynamic behavior has been an important topic in the aeroelasticity study of aircraft for nearly half a century. In this paper, a piecewise optimization describing function (PODF) method is proposed to investigate the characteristics and mechanisms of the free-play-induced complex aeroelastic response. The piecewise expressions of the time history and phase portrait of the limit cycle oscillation are derived by the PODF method, which is helpful to understand the mechanism of the free-play-induced limit cycle oscillation. Another advantage of the PODF method is the ability to predict the higher-order harmonics, which is not possible with the traditional describing function method. In order to verify the validity of the PODF method, a three-dimensional all-movable horizontal tail model with torsion free-play was designed and wind tunnel tests were conducted. The wind tunnel test results are in very good agreement with the calculation results, which proves the effectiveness of the PODF method. In addition, the effect of initial parameters on the dynamic response characteristics is also analyzed using the PODF method. The methodology and conclusions of this paper can provide a reference for the study of nonlinear aeroelasticity and the design of all-movable horizontal tails.

Keywords: free-play, all-movable horizontal tail, limit cycle oscillation, describing function method

## 1. Introduction

Structural nonlinearity has been one of the most important topics of aeroelastic research in recent decades [1-3]. In many aircraft structures, the drive mechanisms inevitably contain friction nonlinearities, bilinear nonlinearities, especially free-play nonlinearities due to gear clearances and loose bearings. Previous studies have shown that aeroelastic system with free-play nonlinearity may exhibit various complex dynamic behaviors, such as bifurcation, chaos, high-order harmonics and limit cycle oscillation, which has a negative impact on handling quality and structural fatigue life [4-8].

Extensive researches have been conducted on the mechanism and characteristics of the free-play-induced limit cycle oscillation [9-12]. Various methods have been developed to study nonlinear aeroelastic behaviors induced by free-play [13-16]. The advantages and disadvantages of these methods are summarized in Table 1.

From Table 1, it is clear that existing methods should be improved to rapidly and accurately predict the complex aeroelastic response caused by free-play. The improved method should have at least the following capabilities: predicting high-order harmonics; reflecting the mechanism of limit cycle oscillation induced by free-play; no iterative computation; no guessing of the initial solution; applicable to three-dimensional models with complex structures; and low computational cost [17-19].

In this paper, the piecewise optimization describing function (PODF) method is proposed to predict the aeroelastic behaviors induced by free-play. The piecewise expressions for the time history and phase portrait of the limit cycle oscillation are derived by the PODF method, and a three-dimensional experimental model with free-play device is designed to verify the PODF method. In addition, the effect of initial parameters on limit cycle oscillation behaviors is investigated.

Table 1 – Characteristics of the main methods for solving free-play nonlinear.

Method	Advantages	Disadvantages
Describing function method	High computational efficiency	Inability to predict high-order harmonics
Higher-order harmonic balance method	Ability to predict high- order harmonics	The expression becomes more complex as the number of harmonics increases
High-dimensional harmonic balance method	Ability to predict high- order harmonics	Requires 2n harmonics to achieve similar accuracy as HOHB method with n harmonics
Numerical continuation method	Ability to perform bifurcation analysis	Not easily suitable for high-DOF systems
<ul><li>Point transformation method</li></ul>	Ability to perform chaos analysis	Only for piecewise linear systems
Hénon's technique	High accuracy	Time-consuming
Precise integration method	High accuracy	Time-consuming

# 2. The Piecewise Optimization Describing Function Method

In this paper, by optimizing the traditional describing function method, the piecewise expressions for the time history and phase portrait of the free-play nonlinear system are derived, and an efficient prediction method for the high-order harmonics is proposed. The PODF method described in this paper includes two steps: 1) Pre-solution based on the traditional describing function method. The traditional describing function method is used to solve the equivalent linearized stiffness of the free-play nonlinear system, and the amplitude and frequency of the limit cycle oscillation at different wind speeds are determined by frequency domain methods such as the PK method; 2) Piecewise optimization of the pre-solution results. The piecewise optimization method is used to solve the time history and phase portrait of limit cycle oscillation, and a fast Fourier transform (FFT) is performed on the time history results to solve the high-order harmonics in the limit cycle oscillation.

The displacement-restoring moment curve of the centrosymmetric free-play is shown in Figure 1. Here:  $\theta$  denotes the angular displacement; F denotes the restoring moment; A denotes the amplitude;  $\delta$  denotes the free-play angle; and  $k_0$  is the stiffness of stiffness region.

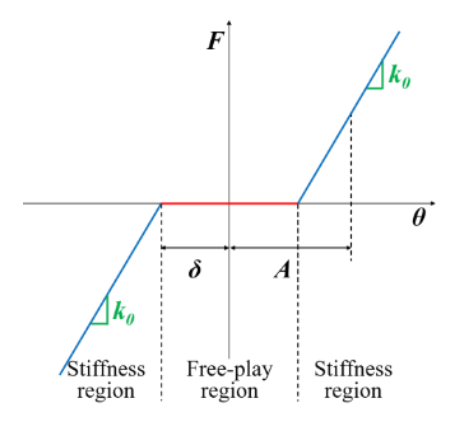


Figure 1 – Symmetric free-play stiffness curve.

The relationship between the angular displacement  $\theta$  and the restoring moment F in Figure 1 can be expressed as a piecewise function:

$$F(\theta) = \begin{cases} k_0(\theta + \delta) & \theta < -\delta \\ 0 & -\delta \le \theta \le \delta \\ k_0(\theta - \delta) & \theta > \delta \end{cases} \tag{1}$$

Related studies have derived the equivalent linearization stiffness  $k^{eq}$ , and the  $k^{eq}$  can be expressed as:

$$k^{eq} = \begin{cases} 0 & A \le \delta \\ k_0 \left[ \frac{2}{\pi} (\varphi - \sin\varphi \cos\varphi) \right] & A > \delta \end{cases}$$
 (2)

$$\varphi = \cos^{-1}\frac{\delta}{A} \tag{3}$$

It follows that  $k^{eq}$  is a constant for any given limit cycle oscillation amplitude and free-play angle. Thus, the free-play nonlinear system can be reduced to a linear system.

When the damping is not taken into account, the aeroelastic equation can be written as:

$$M\ddot{q} + Kq = Q \tag{4}$$

Where:  $\emph{\textbf{M}}$  denotes the generalized mass matrix,  $\emph{\textbf{q}} = [q_1 \cdots q_n \cdots q_m]^T$  denotes the generalized coordinates,  $\emph{\textbf{K}} = \mathrm{diag}(k_{11}, \cdots, k_{nn}^{eq}, \cdots, k_{mm})$  denotes the equivalent linearized stiffness matrix, and  $\emph{\textbf{Q}} = [Q_1 \cdots Q_n \cdots Q_m]^T$  denotes the generalized aerodynamic force matrix.

Solving the aerodynamic forces using the subsonic doublet lattice method requires a reasonable aerodynamic mesh of the lifting surface, as shown in Figure 2.

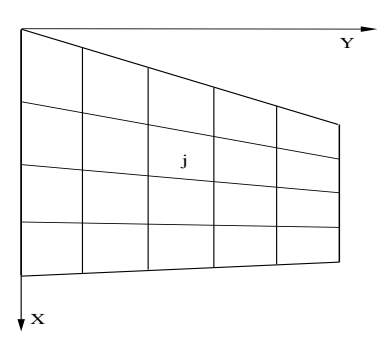


Figure 2 – Schematic of aerodynamic mesh.

Assuming that the lifting surface is divided into n grids and the pressure dipoles are arranged at the pressure points of each grid, the following integral equations are satisfied at the downwash control points under each grid:

$$w_{i} = \frac{1}{8\pi} \sum_{j=1}^{n} \Delta c_{p_{j}} \Delta x_{j} \cos \varphi_{j} \int_{l_{i}} K_{ij} dl_{j} \quad (i = 1, 2, \dots, n; j = 1, 2, \dots, n)$$
 (5)

Where:  $w_i$  denotes the downwash speed at the downwash control point of the ith grid,  $\Delta c_{p_j}$  denotes the pressure coefficient on the jth grid,  $\Delta x_j$  denotes the mid-profile length of the jth grid,  $\varphi_j$  denotes the backward swept angle of the jth grid,  $l_j$  denotes the length of span passing through the pressure point of the jth grid, and  $K_{ij}$  denotes the kernel function.

The above equation can be written in matrix form:

$$\Delta \boldsymbol{p} = \frac{1}{2} \rho V^2 \boldsymbol{D}^{-1} \boldsymbol{w} \tag{6}$$

Where:  $\Delta p = [\Delta p_1 \ \Delta p_2 \ \cdots \ \Delta p_n]$  denotes the pressure distribution array at the pressure point,  $\rho$  denotes the fluid density, V denotes the relative airflow speed, D denotes the matrix of aerodynamic influence coefficients, and W denotes the downwash speed array at the downwash control point. And there are:

$$\Delta p_j = \frac{1}{2} \rho V^2 \Delta c_{p_j} \tag{7}$$

$$D_{ij} = \frac{\Delta x_j}{8\pi} \cos\varphi_j \int_i K_{ij} dl_j \quad (i = 1, 2, \dots, n; j = 1, 2, \dots, n)$$
(8)

The following relationship exists between the downwash speed at the downwash control point and the vibration modes:

$$\mathbf{w} = \left(\frac{\partial \mathbf{F}}{\partial x} + i \frac{k}{h} \mathbf{F}\right) \mathbf{q} \tag{9}$$

Where:  $F = [f_1 f_2 \cdots f_n]$  denotes the modal matrix at the downwash control point, k denotes the reduced frequency, and b denotes the reference semi-chord.

According to the generalized aerodynamic definition, there are:

$$\mathbf{Q} = \mathbf{F}_{P}^{\mathrm{T}} \mathbf{S} \Delta \mathbf{p} \tag{10}$$

Where:  $F_p$  denotes the modal matrix at the pressure point and  $S = \text{diag}(\Delta S_1, \Delta S_2, \dots, \Delta S_n)$  denotes the area weighted array.

Combining the above equations has:

$$\mathbf{Q} = \frac{1}{2}\rho V^2 A \mathbf{q} \tag{11}$$

where A denotes the matrix of generalized aerodynamic influence coefficient:

$$\mathbf{A} = \mathbf{F}_{P}^{\mathrm{T}} \mathbf{S} \mathbf{D}^{-1} \left( \frac{\partial \mathbf{F}}{\partial x} + \mathrm{i} \frac{k}{b} \mathbf{F} \right) \tag{12}$$

Associate equation 4 and equation 11:

$$\mathbf{M}\ddot{\mathbf{q}} + \mathbf{K}\mathbf{q} = \frac{1}{2}\rho V^2 \mathbf{A}\mathbf{q} \tag{13}$$

The above equation can be solved by PK method by setting the free vibration equation of motion as:

$$q = q_0 e^{pt} \tag{14}$$

$$p = \omega(\gamma + i) \tag{15}$$

Where  $q_0$  denotes the initial moment coordinates, t denotes the time,  $\omega$  denotes the circular frequency, and  $\gamma$  denotes the transient decay rate coefficient.  $\omega$  versus the frequency f and  $\gamma$  versus the structural damping coefficient g can be expressed as follows:

$$\omega = 2\pi f \tag{16}$$

$$g = 2\gamma \tag{17}$$

In the vicinity of the critical speed of flutter, the free vibration is close to the simple harmonic vibration, so in the calculation of the aerodynamic force, the non-constant aerodynamic force expression for the simple harmonic vibration is still used.

The expression for the reduced frequency is:

$$k = \frac{\omega b}{V} \tag{18}$$

The reduced frequency can also be expressed as:

$$k = \frac{b}{V} \operatorname{Im}(p) \tag{19}$$

When the system undergoes simple harmonic vibration:

$$\ddot{\mathbf{q}} = -\omega^2 \mathbf{q} \tag{20}$$

From equation 14, there is:

$$\ddot{\boldsymbol{q}} = p^2 \boldsymbol{q} \tag{21}$$

The equation of PK method is:

$$\left(p^2 \mathbf{M} - \frac{p\rho bVIm[\mathbf{A}]}{2k} + \mathbf{K} - \frac{1}{2}\rho V^2 Re[\mathbf{A}]\right) \mathbf{q_0} = \mathbf{0}$$
 (22)

Equation 22 can be expressed as:

$$[R - pI]\overline{q}_0 = 0 \tag{23}$$

$$\mathbf{R} = \begin{bmatrix} \mathbf{0} & \mathbf{I} \\ -M^{-1} \left( \mathbf{K} - \frac{1}{2} \rho V^2 \operatorname{Re}[\mathbf{A}] \right) & \frac{\rho b V M^{-1} Im[\mathbf{A}]}{2k} \end{bmatrix}$$
(24)

Thus, solving Equation 24 can be translated into solving for the eigenvalues of  $\mathbf{R}$ . For a given fluid density, Mach number, and a range of wind speeds, the PK method solves by iterative means for g and f at each wind speed. Thus, the critical wind speed and frequency of the equivalent linearization system can be identified from the V-g diagram and V-f diagram, which can be regarded as the limit cycle oscillation critical values.

Figure 3 show the time history of limit cycle oscillation of the nonlinear system with free-play, including the free-play region (red line) and two stiffness regions (blue line).

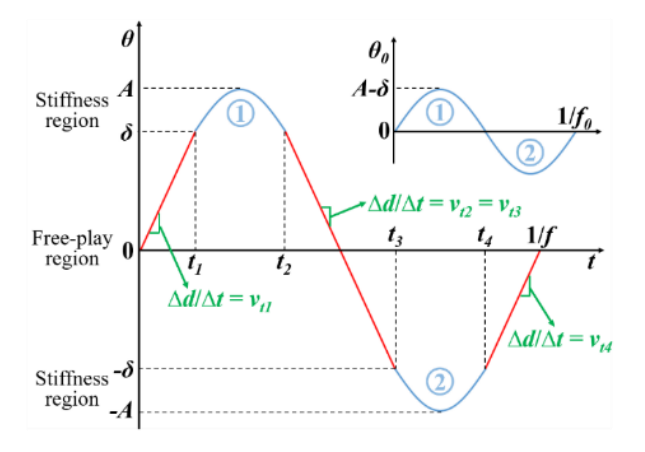


Figure 3 – The time history of PODF method.

The potential energy of the system is 0 at the free-play region and the speed of motion is constant without considering the aerodynamic work. The combination of two stiffness regions can be regarded as a linear system undergoing simple harmonic oscillation (the amplitude is  $A - \delta$ ; the frequency is temporarily set to  $f_0$ ) [20]. The displacement  $\theta_0$  as a function of time t is given by:

$$\theta_0(t) = (A - \delta) \times \sin 2\pi f_0 t \tag{25}$$

The derivative of the above equation has:

$$\dot{\theta}_0(t) = 2\pi f_0(A - \delta) \times \cos 2\pi f_0 t \tag{26}$$

Then:

$$v_{t1} = \dot{\theta}_0(0) = 2\pi f_0(A - \delta) \tag{27}$$

$$v_{t1} = -v_{t2} = -v_{t3} = v_{t4} (28)$$

Where  $v_{ti}$  denotes the speed of motion at  $t_i$ .

Thus there is:

$$\frac{1}{f} = 4 \frac{\delta}{v_{t1}} + \frac{1}{f_0} \tag{29}$$

Combined equations 27 and 29:

$$f_0 = \frac{2\delta + A\pi - \delta\pi}{A\pi - \delta\pi} f \tag{30}$$

$$v_{t1} = (4\delta + 2A\pi - 2\delta\pi)f\tag{31}$$

Thus, the piecewise expressions of the time history can be represented as:

$$\theta(t) = \begin{cases} (4\delta + 2A\pi - 2\delta\pi)ft & 0 \le t \le t_1 \\ (A - \delta) \times \sin\left[\frac{2\pi f(2\delta + A\pi - \delta\pi)(t - t_1)}{A\pi - \delta\pi}\right] + \delta & t_1 \le t \le t_2 \\ -(4\delta + 2A\pi - 2\delta\pi)f\left(t - \frac{1}{2f}\right) & t_2 \le t \le t_3 \\ -(A - \delta) \times \sin\left[\frac{2\pi f(2\delta + A\pi - \delta\pi)(t - t_3)}{A\pi - \delta\pi}\right] - \delta & t_3 \le t \le t_4 \\ (4\delta + 2A\pi - 2\delta\pi)f\left(t - \frac{1}{f}\right) & t_4 \le t \le \frac{1}{f} \end{cases}$$
(32)

$$t_{1} = \frac{\delta}{(4\delta + 2A\pi - 2\delta\pi)f}$$

$$t_{2} = \frac{1}{2f} - \frac{\delta}{(4\delta + 2A\pi - 2\delta\pi)f}$$

$$t_{3} = \frac{1}{2f} + \frac{\delta}{(4\delta + 2A\pi - 2\delta\pi)f}$$

$$t_{4} = \frac{1}{f} - \frac{\delta}{(4\delta + 2A\pi - 2\delta\pi)f}$$
(33)

According to the calculated time histories, the high order harmonics can be computed rapidly by the FFT.

In the same way, the phase portrait of PODF method is illustrated in Figure 4 and can be represented as:

$$v(\theta) = \begin{cases} \pm \sqrt{\left[ (A - \delta)^2 - (\theta + \delta)^2 \right]} \times \frac{2\pi f(2\delta + A\pi - \delta\pi)}{A\pi - \delta\pi} & \theta < -\delta \\ \pm (4\delta + 2A\pi - 2\delta\pi)f & -\delta \le \theta \le \delta \\ \pm \sqrt{\left[ (A - \delta)^2 - (\theta - \delta)^2 \right]} \times \frac{2\pi f(2\delta + A\pi - \delta\pi)}{A\pi - \delta\pi} & \theta > \delta \end{cases}$$
(34)

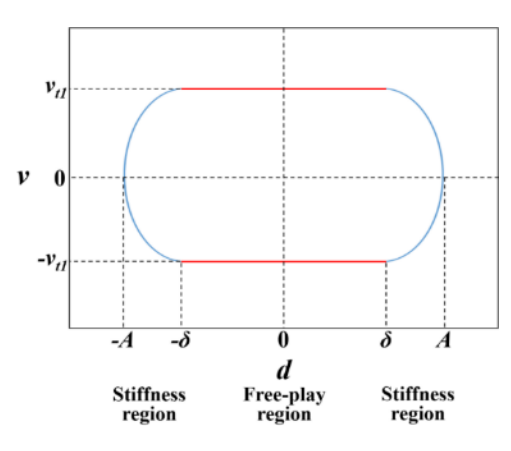


Figure 4 – The phase portrait of PODF method.

## 3. Calculations and Discussion

All-movable horizontal tail systems have complex transmissions. Bearing machining errors, gear clearance, and hinge wear result in the inevitable presence of free-plays in transmissions. Previous studies have shown that the existence of free-play nonlinearity in all-movable horizontal tail leads to

the occurrence of limit cycle oscillation at a speed lower than the critical flutter speed of a linear system, causing problems such as structural fatigue, degradation of maneuvering capability, reduction of aiming accuracy, and structural damage [2]. Therefore, in this section, an all-movable horizontal tail model with torsion free-play is constructed, and the PODF method is used to analyze the effect of free-play nonlinearity on the aeroelastic response of all-movable horizontal tail.

A finite element (FE) model of the all-movable horizontal tail was developed, as shown in Figure 5. Therefore, equation (24) can be solved directly by the FE method, and the time histories and phase portrait can be derived from equations (32) and (34). Thus, the PODF method can be effectively applied to any complex three-dimensional model in conjunction with the FE method [20].

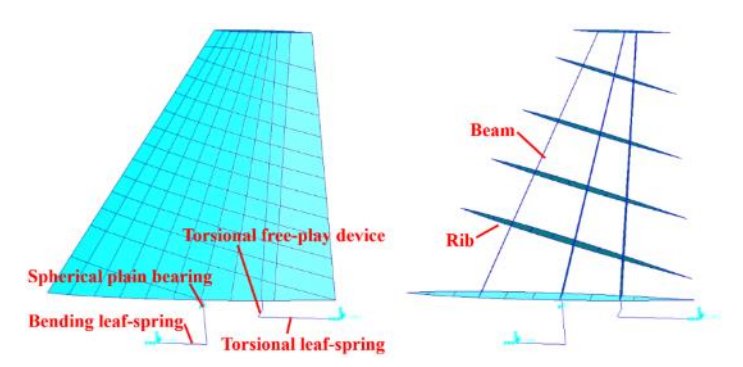


Figure 5 – The finite element model.

Four different torsion free-play angles ( $\pm 0.2^{\circ}$ ,  $\pm 0.4^{\circ}$ ,  $\pm 0.6^{\circ}$ , and  $\pm 0.8^{\circ}$ ) were selected, and the time histories, phase portraits, and frequency spectra of the limit cycle oscillations occurring at 30 m/s and 40 m/s were calculated.

The time histories at different free-play angles and wind speeds are shown in Figure 6. From the figure, it can be seen that the limit cycle oscillation amplitude increases with the free-play value at the same wind speed, and the limit cycle oscillation amplitude increases with the wind speed at the same free-play value. The frequency of the limit cycle oscillation increases with increasing wind speed, independent of the free-play value.

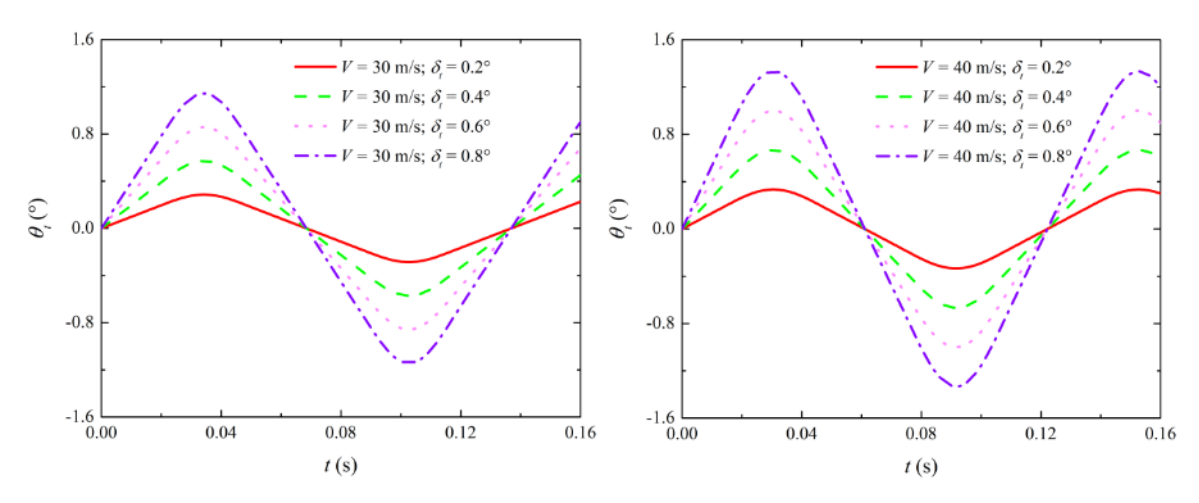


Figure 6 – Time histories at different free-play angles and wind speeds.

The speed-displacement phase diagrams for different initial conditions are shown in Figure 7. From the figure, it can be seen that the vibration angular speed reaches an extreme value in the free-play section, which increases with the free-play value at the same wind speed, and increases with the wind speed at the same free-play value.

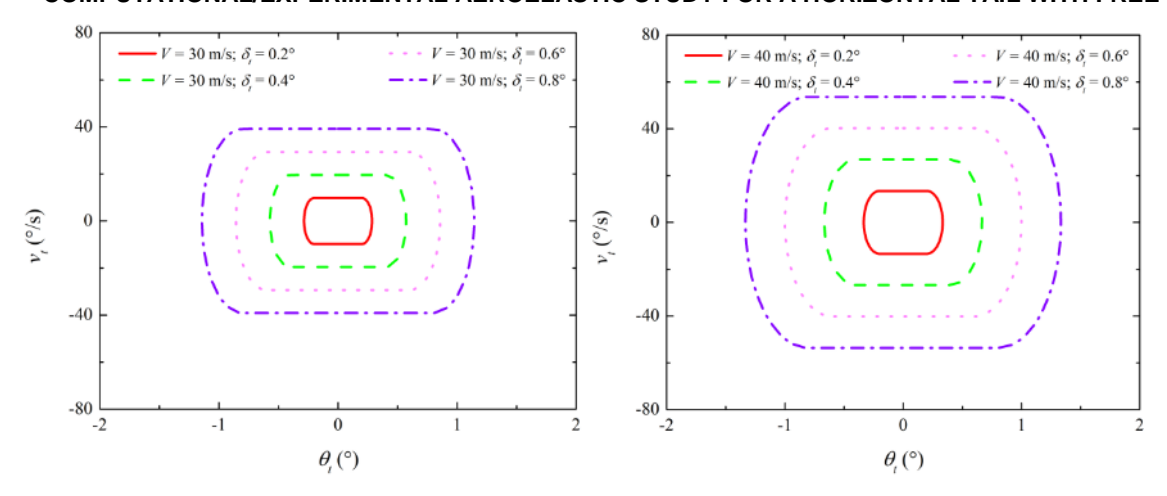


Figure 7 – Phase diagrams at different free-play angles and wind speeds.

The frequency spectra of the limit cycle oscillation for different initial conditions are shown in Figure 8. The high-order harmonics are observed in all eight sets of calculations, and the frequencies of the high-order harmonics are all three times the main frequency. The frequencies of the main frequency and the high-order harmonics increase with increasing wind speed, independent of the free-play value. The peak amplitude of the main and high-order harmonics at the same wind speed increases with the free-play value, and the peak amplitude of the main and high-order harmonics at the same free-play value increases with the wind speed.

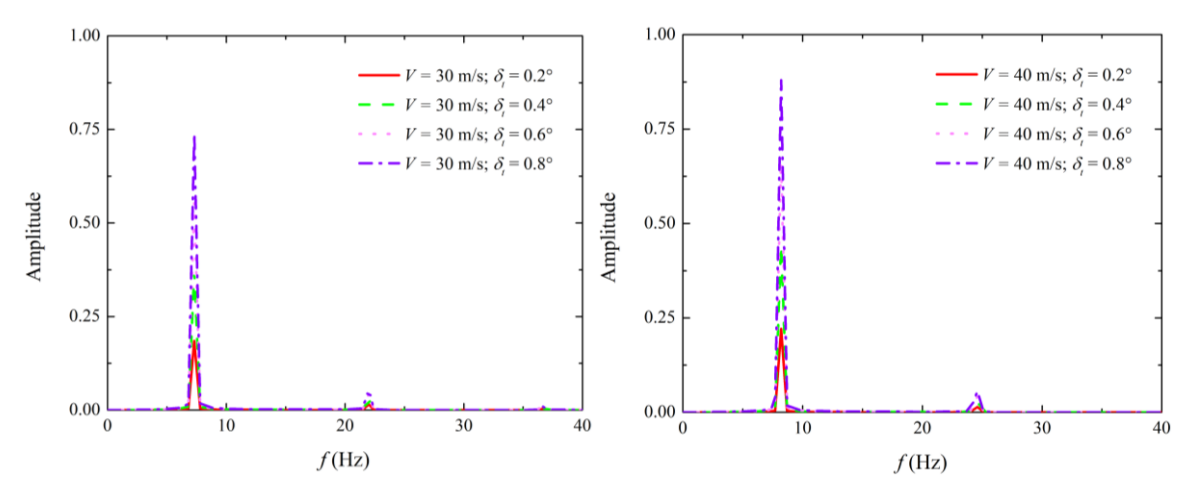


Figure 8 – Frequency spectra at different free-play angles and wind speeds.

# 4. Correlation Between Theory and Experiment

In this section, the PODF method is experimentally validated by wind tunnel tests. The computational results are compared with the wind tunnel test measurements to verify the effectiveness of the PODF method for solving the time history, phase portrait and high-order harmonics of complex three-dimensional structures.

The structure of the wind tunnel test model is consistent with the finite element model. In addition, the fairing and support structure were constructed, as shown in Figure 9. The torsion free-play angle of the wind tunnel test model was measured as  $\pm 0.243^{\circ}$  [20].



Figure 9 – The wind tunnel test model [20].

# 4.1 Time history

The time history of limit cycle oscillation is shown in Figure 10 (i.e. V = 33 m/s is taken as an example). Consistent experimental and computational results demonstrate the effectiveness of the PODF method.

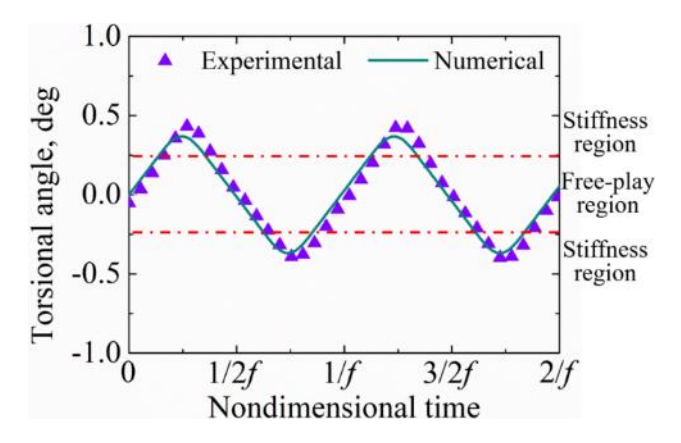


Figure 10 – Time history of torsion angle [20].

# 4.2 Phase portrait

Figure 11 show the phase portrait of limit cycle oscillation. It can be seen that the results of the consistency between the calculations and the wind tunnel tests reconfirm the accuracy of the PODF method.

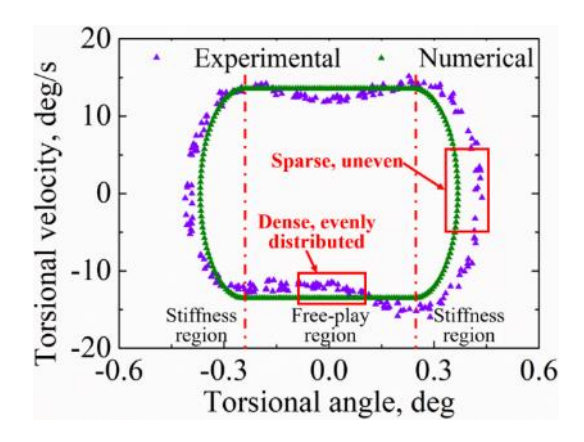


Figure 11 – The phase portrait of the torsion angle and torsion speed [20].

## 4.3 High-order Harmonics

The FFT frequency spectrum is shown in Figure 12. The wind tunnel test results and the computational results show good agreement both in terms of frequency values and the corresponding amplitude response. The 3rd harmonics are observed in both wind tunnel test results and computational results. The PODF method has an advantage over the traditional describing

function method in accurately predicting higher order harmonics.

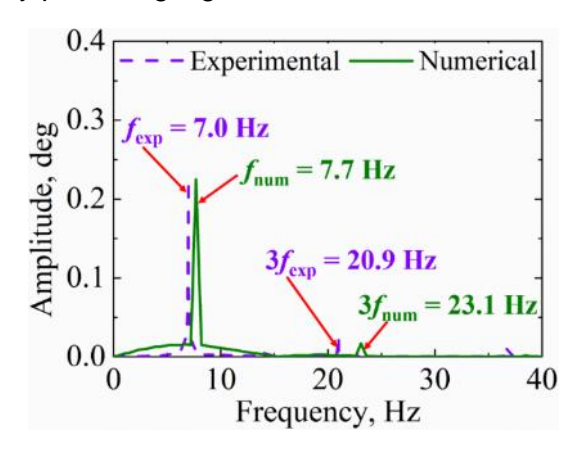


Figure 12 – Frequency spectrum of limit cycle oscillation [20].

# 5. Conclusions

In this paper, a piecewise optimization describing function (PODF) method is proposed to solve the problem that the traditional describing function method cannot predict the high-order harmonics. The PODF method can give the piecewise expressions of the time history and phase portrait of the free play nonlinear system in the limit cycle oscillation process. In the paper, a FE model of all-movable horizontal tail with torsion free play is constructed, and the dynamic behavior of nonlinear aeroelastic systems is studied by the PODF method. In order to verify the effectiveness of the PODF method, a wind tunnel test model with torsion free play is also designed. The results of the wind tunnel test are in good agreement with the simulation results, which proves that the proposed PODF method can accurately predict the time history and phase portrait of the limit cycle oscillation, and the PODF method can also effectively predict the high-order harmonics of limit cycle oscillation. The accuracy of the PODF method is better than that of traditional describing function method. The PODF method improves the shortcomings of traditional describing function method which cannot predict high order harmonics and cannot directly reflect the mechanism of nonlinear aeroelastic behavior induced by free play. In addition, the PODF method has the advantages of the traditional describing function method, such as high computational efficiency, strong applicability and convenient formula derivation.

# 6. Contact Author Email Address

Mailto: qianwei@dlut.edu.cn

# 7. Copyright Statement

The authors confirm that they, and/or their company or organization, hold copyright on all of the original material included in this paper. The authors also confirm that they have obtained permission, from the copyright holder of any third party material included in this paper, to publish it as part of their paper. The authors confirm that they give permission, or have obtained permission from the copyright holder of this paper, for the publication and distribution of this paper as part of the ICAS proceedings or as individual off-prints from the proceedings.

## References

- [1] Bethi RV, Gali SV and Venkatramani J. Response analysis of a pitch–plunge airfoil with structural and aerodynamic nonlinearities subjected to randomly fluctuating flows. *J Fluids Struct*, Vol. 92, pp 102820, 2020.
- [2] Ai X, Bai Y, Qian W, et al. Experimental aeroelastic investigation of an all-movable horizontal tail model with bending and torsion free-plays. *Aerospace*, Vol. 10, pp 434,2023.
- [3] Li W, Zhao D, Zhang L, et al. Proper orthogonal and dynamic mode decomposition analyses of nonlinear combustion instabilities in a solid-fuel ramjet combustor. *Thermal Science and Engineering Progress*, Vol. 27, pp 101147,2022.
- [4] Ma ZS, Wang B, Zhang X, et al. Nonlinear system identification of folding fins with freeplay using direct parameter estimation. *Int J Aerospace Eng*, pp 3978260,2019.
- [5] Tian W, Yang Z and Zhao T. Nonlinear aeroelastic characteristics of an all-movable fin with freeplay and aerodynamic nonlinearities in hypersonic flow. *Int J Non-Linear Mech*, Vol. 116, pp 123-139,2019.
- [6] Chen PC, Ritz E, and Lindsley N. Nonlinear flutter analysis for the scaled F-35 with horizontal-tail free play. *J Aircr*, Vol. 51, No. 3, pp 883-889,2014.
- [7] Banazadeh A and Hajipouzadeh P. Using approximate similitude to design dynamic similar models. *Aerosp Sci Technol*, Vol. 94, pp 105375,2019.
- [8] Tang D and Dowell EH. Aeroelastic response induced by free play, part 2: theoretical/experimental correlation analysis. *AIAA J*, Vol. 49, No. 11, pp 2543-2554,2011.
- [9] Padmanabhan MA and Dowell EH. Gust response computations with control surface freeplay using random input describing functions. *AIAA J*, Vol. 58, No. 7, pp 2899-2908, 2020.
- [10]Wayhs-Lopes LD, Dowell EH and Bueno DD. Influence of friction and asymmetric freeplay on the limit cycle oscillation in aeroelastic system: an extended Hénon's technique to temporal integration. *J Fluids Struct*, Vol. 96, pp 103054,2020.
- [11] Verstraelen E, Dimitriadis G, Rossetto GDB, et al. Two-domain and three-domain limit cycles in a typical aeroelastic system with freeplay in pitch. *J Fluids Struct*, Vol. 69, pp 89-107,2017.
- [12] Chen Y, Chen D and Liu J. Subcritical limit cycle in airfoil aeroelastic system with freeplay: prediction and mechanism. *AIAA J*, Vol. 57, No. 10, pp 4482-4489,2019.
- [13]Yang Z, He S and Gu Y. Transonic limit cycle oscillation behavior of an aeroelastic airfoil with free-play. *J Fluids Struct*, Vol. 66, pp 1-18,2016.
- [14] Tian W, Yang Z and Gu Y. Dynamic analysis of an aeroelastic airfoil with freeplay nonlinearity by precise integration method based on Padé approximation. *Nonlinear Dyn*, Vol. 89, pp 2173–2194,2017.
- [15]He S, Yang Z and Gu Y. Nonlinear dynamics of an aeroelastic airfoil with free-play in transonic flow. *Nonlinear Dyn*, Vol. 87, pp 2099–2125,2017.
- [16]Dai H, Yue X, Yuan J, et al. A comparison of classical Runge-Kutta and Henon's methods for capturing chaos and chaotic transients in an aeroelastic system with freeplay nonlinearity. *Nonlinear Dyn*, Vol. 81, pp 169-188, 2015.
- [17] Afonso F, Coelho M, Vale J, et al. On the design of aeroelastically scaled models of high aspect-ratio wings. *Aerospace*, Vol. 7, pp 116,2020.
- [18]Di Leone D, Lo Balbo F, De Gaspari A, et al. Model updating and aeroelastic correlation of a scaled wind tunnel model for active flutter suppression test. *Aerospace*, Vol. 8, pp 334,2021.
- [19]Wang X, Wu Z, Sun Y, et al. A novel method for estimating three-domain limit cycles in a 3D wing-aileron model with freeplay in aileron deflection. *J Fluids Struct*, Vol. 105, pp 103286,2021.
- [20]Ai X, Bai Y, Qian W, et al. Aeroelastic investigation on an all-movable horizontal tail with free-play nonlinearity. *J Low Freq Noise V A*, Vol. 43, No. 2, pp 634-650, 2024.